IN-SITU DETERMINATION OF THERMAL INERTIA ON NEAR EARTH ASTEROID (162173) RYUGU USING MARA - THE MASCOT RADIOMETER, M. Grott[1] (Matthias.Grott@dlr.de), J. Knollenberg[1], M. Hamm[1], K. Ogawa[2], R. Jaumann[1], K. Otto[1], K. D. Matz[1], N. Schmitz[1], A. Koncz[1], F. Trauthan[1], H. Senshu[3], T. Okada[4], E. Kührt[1], J. Biele[5], W. Neumann[6], M. Knapmeyer[1], J. Helbert[1], A. Maturilli[1], N. Müller[1], A. Hagermann[7], N. Sakatani[4], S. Tanaka[4], T. Arai[4], S. Mottola[1], I. Pelivan[1], L. Drube[1], J.-B. Vincent[1], M. Delbo[8], P. Michel[8], H. Yano[4], C. Pilorget[9], M. Schlotterer[10], C. Krause[11], T.-M. Ho[10], A. Moussi-Soffys[12], [1]German Aerospace Center (DLR), Berlin, Germany, [2]Department of Planetology, Graduate School of Science, Kobe University, Kobe, Japan, [3]Planetary Exploration Research Center, Chiba Institute of Technology, Narashino, Japan, [4]Institute of Space and Astronautical Science, Japan Aerospace Exploration Agency, Sagamihara, Japan, [5]German Aerospace Center (DLR), Cologne, Germany, [6]Institut für Planetologie, University of Münster, Münster, Germany, [7]Univ. Stirling, Stirling, UK, [8]Université Côte d'Azur, Observatoire de la Côte d'Azur, CNRS, Laboratoire Lagrange, Nice, [9]Institut d'Astrophysique Spatiale, Université Paris Sud, Orsay, France, [10]German Aerospace Center (DLR), Bremen, Germany, [11]German Aerospace Center (DLR), Cologne, Germany., [12]Centre National d'Etudes Spatiales (CNES), France.

Introduction: On October 3rd, 2018 the Hayabusa2 spacecraft [1] delivered the MASCOT lander [2] to the surface of near Earth asteroid (162173) Ryugu, where it operated for 17 hours and 7 min. Ryugu has a diameter of 850-880 m, a geometric V-band geometric albedo between 0.042 and 0.055, a bond albedo of 0.019±0.003, and is classified as a Cg taxonomic type [3]. During the surface mission, MASCOT investigated a site located at geophysical coordinates 22.22 ± 0.05°S, 317.26 ± 0.07°E using its magnetometer, near infrared spectrometer, optical camera [4], and radiometer [5].

The MASCOT radiometer MARA [5] obtained surface brightness temperature measurements at the site for a full day-night cycle. Because the scene observed by MARA was also imaged by the optical camera important context information was obtained. MARA observed a rock formation of approximately 60 cm diameter, which is shown in Fig. 1. The projected field of view of the MARA 8-12 µm sensor is indicated in red. The rock has a relatively rough surface and appears angular to subangular.

Data: MARA obtained surface brightness temperature measurements in 6 wavelength bands, but only the 8-12 µm and >3 µm sensors have sufficiently high signal to noise for modeling nighttime temperatures. Surface brightness temperature uncertainties for these filters are estimated to be <2 K at the 2-σ level. The data obtained by MARA is shown in Fig 2a), where surface brightness temperature as determined using the 8-12 µm channel is shown in black together with the 2-σ uncertainty interval in gray.

Modeling: Surface temperatures have been modeled using an asteroid surface thermal model (ASTM) [6] solving the one-dimensional heat conduction equation for a given surface thermal inertia Γ, albedo A, and emissivity ε using

$$-\Gamma\sqrt{\frac{\pi}{P}}\frac{\partial T}{\partial z} = (1-A)I - \sigma\varepsilon T^4 + f\sigma\varepsilon T_{obs}^4$$

as the surface boundary condtion. Here, P is rotation period, T is surface temperature, z is depth normalized to the diurnal skin depth, I is insolation, and σ the Stefan-Boltzmann constant. Emissivity has been varied between 0.9 and 1 and insolation was varied to account for all possible orientations of the surface in the field of view. Reradiation from the surroundings was taken into account by estimating the view factor f to the surrounding environment, which radiates at temperature T_{obs}. View factors f have been varied between 0 and 0.08 as derived from a regional terrain model. The best fitting thermal model is shown in red in Fig. 2a).

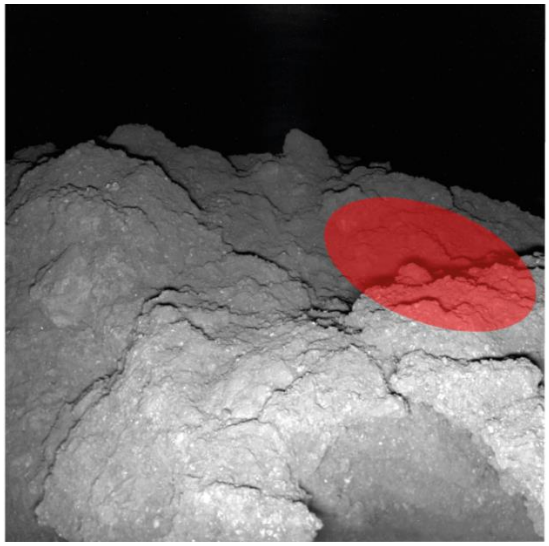

Figure 1 *Projection of the radiometer field of view (red ellipse) onto the scene imaged by MASCOT's optical camera. Nighttime image illuminated by the camera's red LED. MARA observes an agular to subangular rock formation. Because of perspective viewing, pixel resolutions vary across the image between approximately 0.2 mm at the bottom and 3 mm near the horizon.*

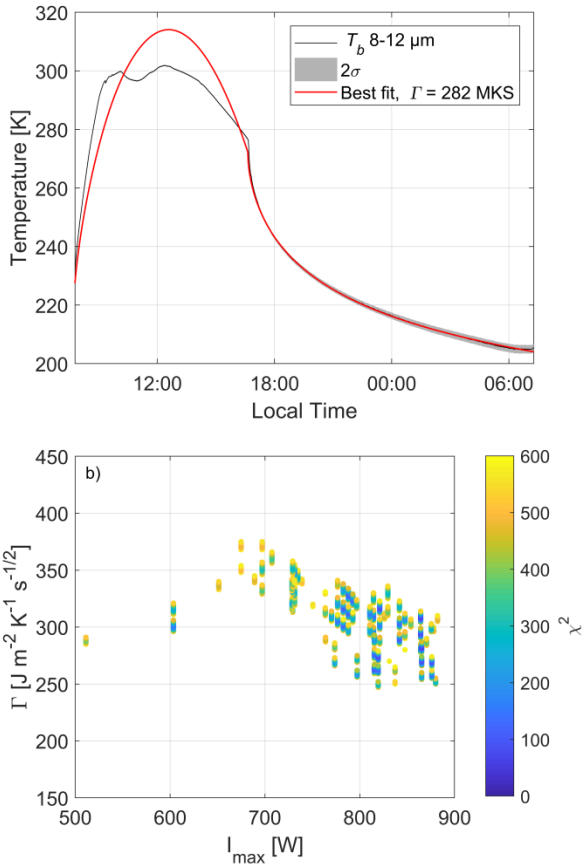

Figure 2 a) *Surface brightness temperatures as a function of local time measured by the MARA 8-12 µm filter indicating the 2-σ confidence limits by shades. Best fitting thermal model is shown in red.* **b)** *Admissible thermal inertia as a function of maximum insolation. The χ^2 of the individual fits is indicated in color.*

While the model excellently fits the nighttime temperatures, the steep temperature increase in the morning as well as the flat shape of the curve around local noon are not reproduced. This is likely due to the complex shape of the surface and its immediate vicinity. A more sophisticated thermal model making use of an accurate digital terrain model would be needed to adequately fit the daytime data. However, it is worth noting that for the given observation geometry, surface roughness would tend to decrease noontime fluxes [7], which would result in better fits for times later than 12:00 local time.

Results: Admissible thermal inertia values for the entire suite of possible illumination conditions are given in Fig. 2b), where thermal inertia is shown as a function of maximum insolation and the χ^2 value of the individual fits is shown in color. As expected, a larger total energy input results in larger model nighttime temperatures, and consequently lower values of the estimated thermal inertia. Overall, admissible thermal inertia ranges from 247 to 375 J m^{-2} K^{-1} s$^{-1/2}$, with a best fitting value of 282 J m^{-2} K^{-1} s$^{-1/2}$.

Discussion: The thermal inertia values determined here are compatible with global estimates derived from telescopic observations [8,3], but much lower than expected from measurements on meteorites in our collections. While thin layers of fine material could in principle mask the thermal signature of competent rock, sand to silt-sized grains have not been observed in camera images and Ryugu generally appears to be deficient in dust and subcentimeter sized particles. Therefore, it seems likely that the boulder observed by MARA exhibits a very low bulk thermal conductivity. However, it cannot be ruled out that the low conductivity zone is limited to a highly porous outer layer, which may for example be generated by cracking due to thermal fatigue [9].

Ryugu's low thermal inertia is in line with observations of comets 67P/CG [10], 9P/Tempel 1, and 103P/Hartley 2 [11,12,13], as well as with estimates based on telescopic observations for C-class asteroid (101955) Bennu [14]. While it was generally accepted that low thermal inertia in the 200 W m^{-1} K^{-1} s$^{-1/2}$ range is indicative of regolith-covered surfaces with particle sizes in the centimeter to sub-centimeter range [3,15], this conclusion needs to be revisited. Results obtained here indicate that even surfaces covered by boulders and block- to slab-sized clasts can exhibit low thermal inertia, which should be taken into account when interpreting thermal infrared data of small bodies such as Ryugu and Bennu. Also, the efficiency of porosity in reducing the thermal inertia of competent blocks remains to be further investigated.

References: [1] Watanabe, S., Tsuda, Y., et al., *Space Sci. Rev.* 208: 3. (2017). [2] Ho, T.M., Baturkin, V., et al., *Space Sci, Rev.* 208: 339, (2017). [3] Wada, K., Grott, M., et al., *Progress Earth Plan. Sci.*, 5:82 (2018). [4] Jaumann, R., Schmitz, N., et al., *Space Sci. Rev.* 208: 375 (2017). [5] Grott, M., Knollenberg, J., et al, *Space Sci. Rev.* 208: 413 (2017). [6] Hamm, M., Grott, M., et al., *Plan. Space Sci.* 159, 1-10 (2018). [7] Giese, B., Kührt, E., Icarus 88, 372-379 (1990). [8] Müller, T.G., Ďurech, J., et al., *A&A* 599: A103 (2017). [9] Delbo M., Libourel, G., et al., *Nature*, 508(7495):233-6 (2014). [10] Spohn, T., Knollenberg, J., et al., *Science* 349: 6247 (2015). [11] Davidsson, B. J. R., Gutiérrez, P. J., Rickmann, H., *Icarus* 201, 335–357 (2009). [12] Lowry, S., Duddy, S.R., et al., *Astron. Astrophys.* 548, A12 (2012). [13] Groussin, O., Sunshine, J.M., et al., *Icarus* 222, 580–594 (2013). [14] Emery, J.P., Fernández, Y.R., et al., *Icarus* 234 17–35 (2014). [15] Gundlach, B., Blum, J., *Icarus* 223, 479–492, (2013).